

## pdf calculations for swirl combustors

**M. S. Anand**

*Allison Engine Co., Indianapolis, IN*

**A. T. Hsu**

*Allison Engine Co., Indianapolis, IN*

**S. B. Pope**

*Cornell Univ., Ithaca, NY*

### **AIAA 34th Aerospace Sciences Meeting and Exhibit, Reno, NV Jan 15-18, 1996**

Calculations are reported for recirculating swirling reacting flows using the joint velocity-scalar probability density function (pdf) method. The pdf method offers significant advantages over conventional finite-volume, Reynolds-average based methods, especially for the computation of turbulent reacting flows. The pdf calculations reported here are based on a newly developed solution algorithm for elliptic flows, and on newly developed models for turbulent frequency and velocity that are simpler than those used in previously reported pdf calculations. Calculations are performed for two different gas-turbine-like swirl combustor flows for which detailed measurements are available. The computed results are in good agreement with experimental data. (Author)

## PDF CALCULATIONS FOR SWIRL COMBUSTORS

M. S. Anand\* and A. T. Hsu  
Allison Engine Company  
P. O. Box 420, Speed Code T-14  
Indianapolis, IN 46206

S. B. Pope#  
Sibley School of Mechanical and Aerospace Engineering  
Cornell University, Ithaca, NY 14853

Calculations are reported for recirculating swirling reacting flows using the joint velocity-scalar probability density function (pdf) method. The pdf method offers significant advantages over conventional finite-volume, Reynolds-average based methods, especially for the computation of turbulent reacting flows. The pdf calculations reported here are based on a newly developed solution algorithm for elliptic flows, and on newly developed models for turbulent frequency and velocity that are simpler than those used in previously reported pdf calculations. Calculations are performed for two different gas-turbine-like swirl combustor flows for which detailed measurements are available. The computed results are in good agreement with experimental data.

### INTRODUCTION

The main advantages offered by the joint velocity-scalar probability density function method for the computation of turbulent reacting flows are that the important processes such as convection by both mean and fluctuating velocities, the effect of turbulence fluctuations on complex multi-step finite-rate reactions, and the effects of reaction/heat release on turbulence appear in closed form and need not be modeled [1]. In conventional finite-volume based Reynolds-averaged approaches, turbulent transport (convection by fluctuating velocities) is modeled using gradient diffusion assumptions (e.g., k-e and Reynolds stress models). More importantly, the conventional models are incapable of accurately accounting for the effect of turbulent fluctuations of species and temperature on mean reaction rates for typical combustion reactions that involve multiple coupled reaction steps and highly nonlinear reaction rates. Further, the effect of heat release and accompanying density fluctuations on turbulence attenuation and turbulent transport are not accurately modeled in conventional methods. Several previous studies reviewed by Pope [2] and more recent studies by Anand et al. [3,4] and Hsu et al. [5] have demonstrated the accuracy and advantages of the pdf method.

The ability to treat turbulent transport and reactions accurately is essential to the accurate predictions of heat release, pollutant formation and other critical characteristics of combustors. Considerable progress has been made through ongoing work at Allison Engine Company in

collaboration with Cornell University towards the development of the pdf method as the next generation gas turbine combustor design and analysis tool. The present work is a significant step in that process.

The present work builds on several past studies [e.g., 3,4,6-10]. The study in Ref. 6 demonstrated the pdf method for elliptic recirculating flows. The pdf method was used in conjunction with a finite-volume method such that the finite-volume method supplied the mean pressure field and the turbulence time scale to the pdf method. The pdf method in turn supplied the Reynolds stresses to the finite-volume method so that conventional turbulence models are avoided. The coupling was needed since the velocity-scalar pdf method used did not include information about the turbulence time scale and although the mean pressure field could be determined from the mean velocity field, a robust algorithm was needed to solve the Poisson equation for pressure which involves the evaluation of second derivatives of mean velocities and other terms with minimal statistical error. Such a pressure algorithm was developed by Anand et al. [7] and demonstrated for elliptic recirculating flows such as the flow over a backward-facing step. The time scale was still supplied externally to the pdf method in that study.

A model for the mean turbulence time scale, rather for the mean turbulence frequency (inverse of the turbulence time scale), was developed and solved in conjunction with the pdf method by Anand et al.[8]. Subsequently a stochastic frequency model was developed by Pope et al.[9,10]. With this model, the turbulent frequency is also considered as a random variable in the joint velocity-scalar-frequency pdf (or the joint velocity-scalar pdf where one of the scalars is the frequency), which would then contain the needed time scale information. These models were used for computing

---

\* AIAA Member

# AIAA Associate Fellow

Copyright © 1996 by authors. Published by AIAA Inc. by permission.

swirling jet flows and swirling jet diffusion flames [3,4]. Due to the nature of the flows calculated, these computations were able to use boundary layer assumptions for determining the pressure gradients and did not require the solution of the elliptic equation for pressure. All the computations mentioned above showed excellent comparison with detailed experimental data including mean velocity and temperature and higher turbulent moments (up to fourth order compared).

The present study represents the first fully self-contained pdf calculations for elliptic flows and incorporates the elliptic flow solution algorithm as well as the stochastic frequency model. However, with a view to making the method more robust, easier to implement and affordable for complex multidimensional flows, a significantly different elliptic flow algorithm (or pressure algorithm) has been developed and implemented. The models for turbulent frequency and velocity have also been considerably simplified.

The newly developed method (elliptic algorithm and models) is validated against benchmark experimental data and previous pdf solutions mentioned above.

#### THE PDF METHOD -- MODELING AND SOLUTION ALGORITHM

The joint pdf  $f(\underline{V}, \underline{\psi}, \eta; \underline{x}, t)$  at position  $\underline{x}$  and time  $t$  is defined as the probability density of the simultaneous event  $\underline{U}(\underline{x}, t) = \underline{V}$ ,  $\varphi(\underline{x}, t) = \underline{\psi}$  and  $\omega(\underline{x}, t) = \eta$ , where  $\underline{U}$  is the velocity vector,  $\varphi$  is a set of scalars,  $\omega$  is the turbulence frequency, and  $\underline{V}$ ,  $\underline{\psi}$  and  $\eta$  are independent variables in the velocity-scalar-frequency space. Starting from the usual conservation equations for mass (continuity), momentum, scalar quantities and turbulent frequency, the transport equation for the joint pdf can be derived as described in Ref. 1. In this equation, the terms involving convection (mean and turbulent), reaction, body forces, and the mean pressure gradient effects (including the variable density effects in those terms) appear in closed form. The terms representing the effects of viscous dissipation, fluctuating pressure gradient, molecular mixing of scalars, and production and dissipation of turbulence frequency need to be modeled. A Lagrangian viewpoint is adopted in modeling and solving the joint pdf equation. The modeled pdf transport equation is solved by the Monte Carlo technique.

In the Monte Carlo solution technique, notional particles representing fluid particles are distributed throughout the solution domain overlaid by a spatial or computational grid. Each particle is attributed with values for its spatial position ( $\underline{x}^*$ ), velocity ( $\underline{U}^*$ ), scalar values ( $\varphi^*$ ) and turbulence frequency ( $\omega^*$ ). These values evolve according to the equations described below which include modeled terms where needed. Starting from arbitrary initial conditions and specified boundary conditions, the particle values are marched in time-steps which are a fraction of a characteristic time scale in the flow until a steady-state solution is reached. The solution of these evolution equations constitutes the solution

of the pdf transport equation. Means of any functions of the independent variables are determined by a sophisticated ensemble averaging procedure (cloud-in-cell estimate using bi-linear basis functions) followed by smoothing using local linear least squares [11]. Additionally time-averaging, with a low time constant initially and a higher value near convergence, is used for mean quantities to further reduce the statistical error.

#### Particle Evolution Equations

The increment  $d\underline{x}^*$  in the position of a particle over an infinitesimal time interval  $dt$  during the time step is given by the exact equation:

$$d\underline{x}^* = \underline{U}^* dt \quad (1)$$

This exact equation causes the mean and turbulent convection to be in closed form.

The model used for the increment in the particle velocity is a variant of the simple Langevin model, and is described by:

$$dU_i^* = -\frac{1}{\rho^*} \frac{\partial \langle P \rangle}{\partial x_i} - \left( \frac{1}{2} + \frac{3}{4} C_0 \right) (U_i^* - \langle U_i \rangle) \Omega dt + (C_0 \Omega k)^{1/2} dW_i \quad (2)$$

where angled brackets denote (density-weighted or Favre) means,  $\langle P(\underline{x}^*) \rangle$  is the mean pressure,  $\langle U_i \rangle$  is the Eulerian mean velocity,  $k$  is the turbulent kinetic energy,  $\Omega$  is the conditional mean turbulence frequency described below,  $\rho^*$  is the particle density,  $C_0$  is a universal constant, and  $dW_i$  represents an isotropic Wiener random process. The first term in Eq. 2 exactly accounts for the acceleration due to mean pressure gradients including variable-density effects. The last two terms together model the effects of viscous dissipation and fluctuating pressure gradient.

The main difference between the current model and the simple Langevin model used previously [e.g. 3, 6-8, 12, 13] is that the conditional mean frequency appears instead of the unconditional mean frequency  $\langle \omega \rangle$ . The conditional mean frequency is the "above-average" mean defined by [14]:

$$\Omega = C_\Omega \langle \omega \mid \omega^* \geq \langle \omega \rangle \rangle \quad (3)$$

i.e., it is proportional to the mean of the instantaneous frequencies that are greater than or equal to the unconditional mean frequency. In intermittent regions where both turbulent ( $\omega > 0$ ) and nonturbulent ( $\omega = 0$ ) fluid exist, the conditional mean frequency is representative of the "frequency in the turbulent fluid" which is the appropriate quantity to be used in modeling the turbulent process. As a consequence of its definition (Eq. 3),  $\Omega$  is larger than  $\langle \omega \rangle$  in such regions. This facilitates the entrainment of nonturbulent particles without requiring additional modeling. (See Ref. 14

for more details.). The constant  $C_\Omega$  (determined in terms of incomplete gamma functions) has the value 0.6893, and is specified such that  $\Omega = \langle \omega \rangle$  in homogeneous turbulence [14].

The value  $C_0 = 2.1$  (determined in Ref. 12) has been used in previous studies for the Langevin model (Eq. 2) that uses the unconditional mean frequency [e.g. 3, 6-8, 12, 13].

A new stochastic model for the evolution of the frequency of the particle ( $\omega^*$ ), developed by Jayesh and Pope [13], has been used in the present study. For the sake of brevity, the model is not presented here. Compared to the previous stochastic frequency model developed by Pope et al. [9, 10], the new model is easier to implement and is expected to be more robust. The new model includes the conditional mean frequency (Eq. 3) and avoids the inclusion of an ad hoc term in the previous model to account for intermittent regions. The evolution of the (unconditional) mean frequency, according to the model, is given by:

$$\left\langle \frac{D\omega}{Dt} \right\rangle = C_1 S_{ij} S_{ij} - C_2 \langle \omega \rangle^2 \quad (4)$$

where left-hand side is the mean rate of change following the fluid, the first term on the right represents the production and the second term represents the decay of  $\langle \omega \rangle$ , and  $S_{ij}$  is the mean rate of strain given by

$$S_{ij} = \frac{1}{2} \left( \frac{\partial \langle U_i \rangle}{\partial x_j} + \frac{\partial \langle U_j \rangle}{\partial x_i} \right) \quad (5)$$

Jayesh and Pope [14] suggest the values  $C_1=0.08$  and  $C_2=0.9$  for the constants in the frequency model.

The evolution of the  $\alpha$ -th species or scalar value of a computational particle is given by

$$d\varphi_{\alpha}^* = S_{\alpha}(\varphi^*) dt - C_{\varphi} (\varphi_{\alpha}^* - \langle \varphi_{\alpha} \rangle) \Omega dt \quad (6)$$

where  $S_{\alpha}(\varphi^*)$  is the reaction rate for the species  $\varphi_{\alpha}$  as a function of the instantaneous composition  $\varphi^*$ , and the second term represents a simple relaxation-to-mean model for molecular mixing of scalars. Therefore, given the reaction rate (determined by the thermochemistry used), the treatment of reaction and the turbulence chemistry interactions are in closed form. The value of the constant  $C_{\varphi}$  for molecular mixing is typically in the range 1.5-2.0.

Due to the differences in the models used in the present study compared to those used in the previous studies discussed above, the values of the model constants used in the present study differ slightly from their standard values.

The time increment,  $\Delta t$ , for each step is chosen to be a fraction ( $=0.1$ ) of the minimum of a) the inverse of the maximum mean turbulence frequency in the computational domain or b) the minimum characteristic time for any particle to cross a computational cell based on the mean and

variance of velocity in the cell. All the particles in the computation are marched with the same time increment. The particle evolution equations are integrated over the time step with an accuracy of second-order or better.

It should be noted that the models described above for velocity, frequency and scalar mixing are all being used in the joint pdf method for the first time to compute general (inhomogeneous, swirling, recirculating) turbulent reacting flows. As such the present study serves to validate the elliptic flow algorithm as well as the models used.

### Elliptic Flow Algorithm (Position, Velocity and Pressure Correction)

The main purpose of the elliptic flow algorithm is to determine the mean pressure field to be used in the velocity equation (Eq. 2) while ensuring that the mean conservation equations for mass and momentum are satisfied. The elliptic flow algorithm newly developed by Pope [15] is used in the present study. The algorithm performs a velocity correction to satisfy mean mass conservation and determines a mean pressure correction on every step starting from arbitrary initial conditions. Variance reduction techniques are applied (i.e. turbulent processes such as mixing, viscous dissipation, etc. are performed on sub-ensembles such that the sub-ensemble means are not changed) so that mean momentum conservation is also maintained. In addition, a correction to the position of the particles are made to ensure that the consistency condition for particle methods, namely that the volume associated with a sub-ensemble of particles should equal the geometric volume occupied by the particles, is satisfied. For statistically stationary flows, a steady state is achieved in which these corrections tend to zero (in the mean, and the variance decreases as the number of particles increases).

In the algorithm a velocity correction potential  $\Phi$  is determined such that after adding the velocity correction

$$\delta \underline{U} = - \frac{1}{\langle \rho \rangle} \nabla \Phi, \quad (7)$$

the corrected velocity field satisfies the continuity equation. ( $\langle \rho \rangle$  is the mean density of the fluid.) When the velocity increment is determined by Eq. 7 for a time step  $\Delta t$ , it is equivalent to the effect of a mean pressure correction

$$\delta \langle P \rangle = \Phi / \Delta t. \quad (8)$$

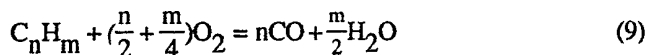
The Poisson equation for the velocity correction potential is set up and solved using bi-linear basis function representation for calculating mean quantities. Thus, the mean pressure field is not determined directly from the solution of the Poisson equation. However, any error in the mean pressure field is compensated by the velocity correction, i.e., the potential  $\Phi$  is such the total effect of the correct pressure should be felt.

In contrast, the pressure algorithm developed and used by Anand et al. [7] solves for the Poisson equation for pressure as well as for the velocity correction potential. However, since the Poisson equation involves second derivatives of mean velocities it is necessary to determine the mean velocity field to a high degree of accuracy. Hence bi-directional cross-validated cubic splines are used to determine means in that algorithm which can be computationally expensive. The current algorithm is expected to be less expensive and more robust. The more important advantage is that it is easier to extend the current algorithm to irregular geometries (body-fitted grids) and to three-dimensional flow calculations.

### Thermochemistry

Hydrogen and methane flames are studied in the present work. A fast equilibrium chemistry model is used for the hydrogen flame calculations because the time scale for hydrogen-air reaction is very small compared to the turbulent time scale. For the hydrogen case, the only scalar variable in the calculations is the mixture fraction. Temperature is also included but is needed for output only. The mixture fraction is a conserved variable (reaction rate is zero). The density and temperature are determined as equilibrium properties from the mixture fraction.

For methane flame calculations, a general 2-step chemistry by Westbrook and Dryer [16] for saturated hydrocarbon fuels is used. The two steps are:



In addition to mixture fraction, two more scalar variables--namely the mass fractions of carbon dioxide and water--are included in the pdf calculations. The temperature and density are determined as functions of these three scalar variables.

For both the fast chemistry and the 2-step chemistry models, lookup tables were created to reduce the CPU requirements of the calculations. In the case of the fast chemistry, a one-dimensional table is created, and for the 2-step chemistry, a three-dimensional table is generated. For the 2-step chemistry calculations, the table is generated for a given specific time increment,  $\Delta t$ , used by the flow calculations ( $\Delta t = 2.5 \times 10^{-5}$  s in the present calculations). In the table generation processes, the NASA CEC thermal data were used to calculate the variable specific heats and the temperature.

### RESULTS AND DISCUSSION

The present pdf method was applied to the (constant-density) flow over a backward-facing step previously

calculated by Anand et al. [7] for which measurements have been reported [17]. As before, the results (not presented here) were in excellent agreement with data for reattachment length, mean velocities and up to third order turbulent correlations measured.

Results are presented for two laboratory swirl combustor configurations which have the essential flow features of gas turbine combustors, namely swirl, recirculation, large velocity gradients, turbulence and combustion. The experiments were conducted by researchers at the University of Dayton Research Institute at the Wright Patterson Air Force Base, Dayton. The velocity measurements were made using a three-component laser Doppler velocimeter (LDV) and temperature measurements were made using coherent anti-Stokes Raman spectroscopy (CARS).

### Swirling Hydrogen Diffusion Flame

Figure 1 shows the schematic of the swirling jet diffusion flame combustor configuration. The test case considered had a central fuel (hydrogen) jet bulk velocity of 100 m/s, the swirling air bulk velocity of 20 m/s and the nonswirling coflow air velocity of 4 m/s. The swirler vane angle was 30 deg. and swirl number for the swirling jet, calculated from the measured velocities, was 0.382. Detailed measurements for mean velocities and turbulent correlations up to fourth order are reported (see references listed in Ref. 4) at several downstream locations starting from the axial location  $x = 1.5$  mm from the nozzle. While no species measurements were made, mean and variance of the temperature are reported at the same locations.

The flow was previously calculated by Anand et al. [4] using a joint pdf method. Since the flow is primarily parabolic in nature (with no recirculation), the pdf solution algorithm was based on boundary-layer assumptions with extensions for swirling flows. The method also used more sophisticated models, namely the stochastic frequency model of Pope [10] in conjunction with the refined Langevin model for velocity [10] in which the instantaneous particle frequency rather than a mean frequency is used in the random term shown in Eq. 2 along with a resulting additional drift term. The reason for calculating the flow with the present method is to not only validate the method and the models but also to assess if the elliptic flow algorithm can better resolve the flow in regions where boundary-layer assumptions (e.g., neglect of axial gradients) are questionable.

The present computations were performed, on an IBM RS6000/370, using a nonuniform grid (31 in  $x$  by 61 along the radius  $r$ ) with about 190 particles per cell. Increasing the nominal number of particles per cell to 290 produced nearly the same results. The inlet boundary conditions were taken from experimental data as described in Ref. 4. Calculations were performed for time 2000 steps.

In the figures to be presented for this case the measured mean axial velocity on the centerline at the nozzle exit,  $\langle U \rangle_{OC}$ , which is 130.3 m/s in this case, is used to normalize

the velocity statistics. The axial distances and radius are normalized by the nozzle diameter,  $D$  ( $= 9.45$  mm) and nozzle radius  $R$  ( $= D/2$ ) respectively. The temperature results are normalized by the stoichiometric temperature,  $T_{st}$  ( $= 2377$  K). For the experimental data presented, the open squares represent data conditioned on the inner fuel jet, the solid circles represent data conditioned on the swirling air jet, and the inverted triangles represent the data conditioned on the outer coflow air.

Figure 2 shows the convergence history for the (unnormalized) mean axial and radial velocities at the monitoring location  $x/D = 10$  and  $r/R = 4$ . The figure shows that the solution has converged and a steady-state has been reached. Typically oscillations are seen during the initial (first few hundred) steps before the solution settles down and reaches a steady state. Also, steady state and convergence were usually achieved by about 1500 steps for both the cases presented here.

Figure 3 shows the radial profiles of normalized mean axial velocity  $\langle U \rangle$  at different downstream locations compared against data. The measurements are conditional on the origin of the fluid and are made by seeding (for LDV) each of the jets (fuel, annulus and coflow) individually. Differences in the velocity statistics for each of the jets can be seen in the data. The pdf method can calculate these conditional values without requiring additional modeling, and such calculations have been presented in Refs. 3 and 4. However, in the present study, only the unconditional quantities are calculated and compared against data. The present results (solid lines) are also compared against results from the boundary-layer (b-l) algorithm (dashed line) [4]. Figure 3 shows that the present results are in excellent agreement with data at all stations. Also, the present calculations are in better agreement with data than the b-l results not only with respect to the overall spreading but also in the near-nozzle region ( $x/D = 1.06$  and  $2.65$ ) where the flow is tending toward recirculation (near  $r/R = 1.5$ ) and the b-l approximations are inaccurate.

Similar observations can be made for the swirl velocity results presented in Figure 4. Although the b-l calculations are in good agreement with data, the present calculations show a better agreement.

The profiles of mean (Reynolds-averaged) temperature,  $\bar{T}$ , presented in Figure 5 show that the transport and mixing of the fuel is well calculated in the present study, resulting in a very good agreement with the temperature data. (Note that CARS measurements are closer to Reynolds-averaged values than density-weighted values [4].) The present results are better than the b-l results at the downstream locations, but near the nozzle (e.g.,  $x/D = 2.65$ ) the present results show a lower peak and a greater spread than the data and the b-l results show. Results for the temperature variance from both the methods (not shown here) were overall in good agreement with data although some differences consistent with their mean temperature profiles were observed.

Profiles for turbulent kinetic energy presented in Figure 6 show that both the calculations are in good agreement with data in the region up to  $x/D = 5.29$  while the b-l calculations overpredict the kinetic energy at downstream locations which is consistent with the lack of spreading in the mean velocity profiles. Sample results from the present calculations for third and fourth order turbulent correlations presented in Figure 7 are in good agreement with data.

Overall, the results are in very good agreement with data, and are as good or better than those obtained with the boundary-layer calculations.

### Methane Step-Swirl Combustor

The step-swirl combustor shown in Figure 8 is an extension of the jet diffusion flame combustor (Figure 1), and is closer to a practical gas turbine combustor. It consists of a central air jet (20 mm diameter) surrounded by an annular fuel tube (29 mm o. d.) which is again surrounded by a swirling air jet (40 mm o. d. taken to be the characteristic diameter  $D$ ). Measurements for this case are reported in Ref. 18. For the case considered here the inner air jet was nonswirling and the outer air had a 30 deg. vane-angle swirler. The bulk velocity for the inner air, fuel and outer air jets are 14.4, 2.5, and 8.6 m/s, respectively.

The velocity data reported for this combustor are also conditional velocities. Unfortunately, the authors [18] were unable to measure the velocities conditional on the outer air jet due to practical difficulties such as the LDV seed particles striking the optical windows and clogging them up. The outer swirling flow has a major effect on the development of the flow and it is crucial to have accurate inlet conditions to accurately simulate the flow. The computations also show high sensitivity to the inlet profiles, especially since the comparison with data is made in the region  $x/D < 2$  up to which measurements were made. In the present study the inflow velocity profiles had to be reconstructed based on existing experimental data and the overall mass flow rates through the different streams.

The computations were performed using a nonuniform  $41 \times 41$  grid using 200 particles per cell. The computations were made for 2000 steps with convergence achieved in most of the flow field by about 1500 steps. The results are presented in Figures 9 through 14. The values used for normalization in the figures are  $\langle U \rangle_{oc} = 21.6$  m/s,  $T_{st} = 2272$  K,  $D = 40$  mm, and  $R = D/2$ . For the experimental data presented, the solid symbols represent data conditioned on the inner air jet and the open symbols represent data conditioned on the fuel jet.

The profiles of mean axial velocity,  $\langle U \rangle$ , presented in Figure 9 show the calculations capture the overall flow features well. Although the recirculation is well predicted, the location and radial extent of the recirculation zone which are very sensitive to the inlet mean radial and swirl velocities assumed for the outer swirling jet, are underpredicted.

The profiles of mean radial velocity,  $\langle V \rangle$ , in Figure 10 show the expected trends although data are not available in the critical regions where the largest radial velocities are present. Note that computed results are unconditional and are expected to be lower than the fuel conditioned radial velocity at the outer edge of the fuel jet as seen at  $x/D = 0.5$ . Figure 11 shows that the mean swirl (or tangential) velocity,  $\langle W \rangle$ , is well predicted both in terms of the peak location and the decay downstream.

The mean temperature profiles presented in Figure 12 predict the shapes of the measured profiles well and for the most part agree in magnitude with the data. The profile of the fuel mass fraction at the inlet significantly influences the temperature distribution at the near-nozzle locations at which comparisons are being made. Although the fuel tube only supplies fuel, considerable mixing takes place even as the fuel is leaving the fuel tube, and an assumption of a plug flow profile leads to a much worse comparison with temperature than with a smooth but sharply peaked profile assumed for the computations shown.

The profiles of turbulent kinetic energy and a fourth order turbulent correlation shown in Figures 13 and 14, respectively, are in reasonably good agreement with data. Overall, the results are in good agreement with data for all the quantities considering the uncertainty in the inlet conditions.

The results for the hydrogen and methane cases have validated the new models and the elliptic flow algorithm used. The calculations represent the first quantitative results from the new code incorporating the algorithm and models. The results compare very well with the detailed data from practical combustors.

#### CONCLUDING REMARKS

Computations using the joint pdf approach have been reported for two swirl combustor configurations. The study uses a newly developed solution algorithm for elliptic flows and new simplified models for velocity and turbulence frequency. The methane combustor calculations represent the first fully self-contained joint pdf calculations for elliptic reacting flows. The results for both combustors are in good agreement with data. The study serves to further validate the joint pdf method and the models, and is a significant step in the development of a pdf-based combustor design system.

The ability of the joint pdf method to accurately calculate the mean and turbulent velocity fields, scalar transport, and temperature using multi-step finite-rate chemistry offers significant advantages for its use in the design of current and future high performance and low emissions gas turbine combustors.

The present results are compared against calculations using the scalar pdf method (in which the joint pdf of only the scalars is considered) and other conventional turbulent combustion models in an accompanying paper [5]. The study

demonstrates the advantages and the superior accuracy of pdf methods, in particular the joint velocity-scalar pdf method.

#### ACKNOWLEDGMENTS

This work is supported in part by the U. S. Air Force, Wright Laboratory, under Contract F33615-87-C-2821. The authors would like to thank the Air Force Technical Monitors Dr. Mel Roquemore and Mr. Jeff Stutrud for their support. The authors would also like to thank Dr. Mohan Razdan of Allison for his support and useful discussions.

#### REFERENCES

1. S. B. Pope, *Progress in Energy and Combustion Science*, 11, p. 119, 1985.
2. S. B. Pope, *Twenty-Third Symposium (International) on Combustion*, The Combustion Institute, Pittsburg, p. 591, 1990.
3. M. S. Anand, S. B. Pope and H. C. Mongia, AIAA 93-0106. To be published in *AIAA Journal*.
4. M. S. Anand, F. Takahashi, M. D. Vangsness, M. D. Durbin and W. J. Schmoll, ASME 95-GT-307, To be published in *The Transactions of the ASME*.
5. A. T. Hsu, M. S. Anand, and M. K. Razdan, AIAA 96-0523, 1996
6. M. S. Anand, S. B. Pope and H. C. Mongia, *Turbulent Reactive Flows*, Lecture Notes in Engineering, 40, p. 672, 1989.
7. M. S. Anand, S. B. Pope and H. C. Mongia, *CFD Symposium on Aeropropulsion*, NASA CP-3078, p. 347, 1990.
8. M. S. Anand, S. B. Pope and H. C. Mongia, *Seventh Symposium on Turbulent Shear Flows*, Stanford University, p. 3.3, 1989
9. S. B. Pope and Y. L. Chen, *Physics of Fluids A*, 2, No. 8, p. 1437, 1990.
10. S. B. Pope, *Physics of Fluids A*, 3, No. 8, p. 1947, 1991.
11. T. D. Dreeben and S. B. Pope, FDA 92-13, Cornell University, Ithaca, NY, 1992.
12. M. S. Anand and S. B. Pope, *Turbulent Shear Flows 4*, eds. L. J. S. Bradbury, et al., Springer-Verlag, p. 46, 1985.
13. D. C. Haworth and S. B. Pope, *Physics of Fluids*, 30, p. 1026, 1987.
14. Jayesh and S. B. Pope, Report FDA 95-05, Cornell University, Ithaca, NY, 1995.
15. S. B. Pope, Report FDA 95-06, Cornell University, Ithaca, NY, 1995.
16. C. K. Westbrook and F. L. Dryer, *Combustion Science and Technology*, 27, 1981.
17. S. W. Pronschick and S. J. Kline, Report MD-42, Stanford University, 1983.
18. M. D. Durbin, M. D. Vangsness, D. R. Ballal, and S. R. Katta, ASME 95-GT-111, 1995

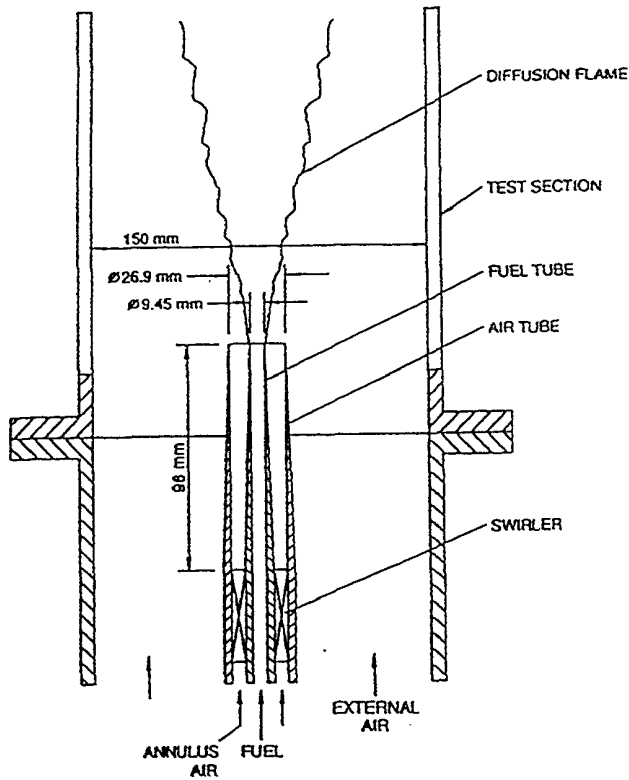


Figure 1: Schematic of the hydrogen swirling jet diffusion flame configuration.

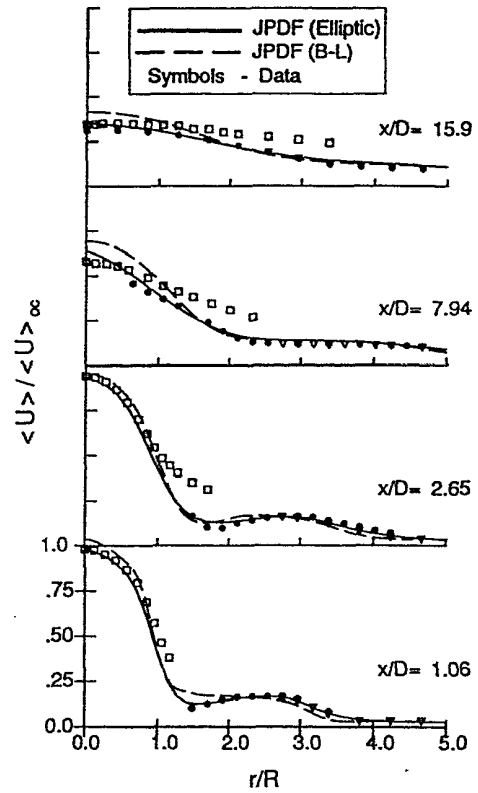


Figure 3: Computed mean axial velocity profiles compared against data for the hydrogen flame.

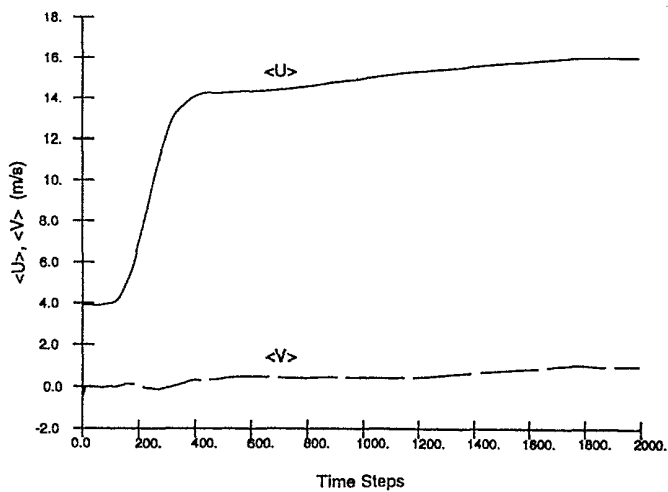


Figure 2: Convergence history for the mean axial and radial velocities for the hydrogen flame computations.

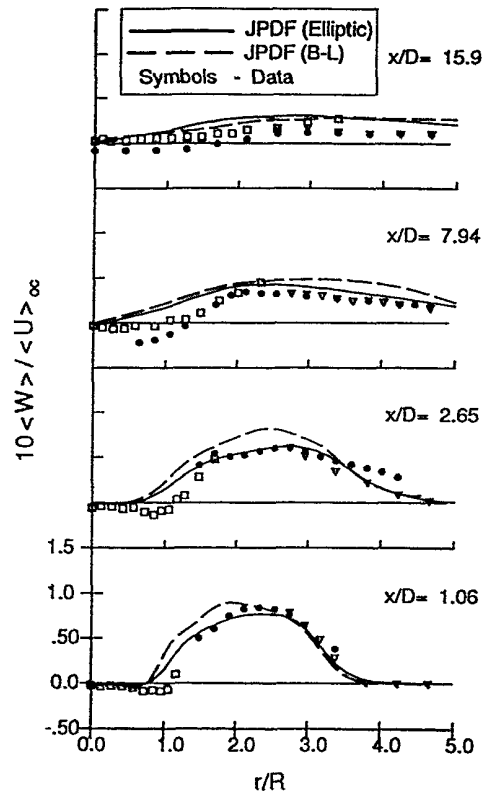


Figure 4: Computed mean swirl velocity profiles compared against data for the hydrogen flame.

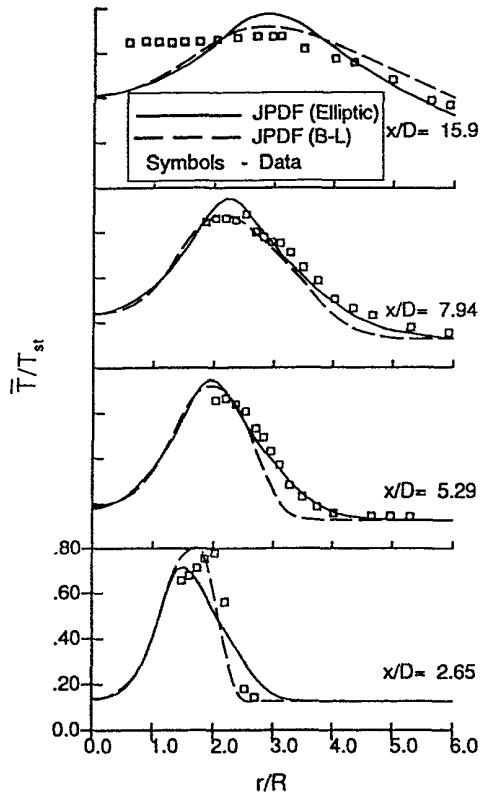


Figure 5: Computed mean temperature profiles compared against data for the hydrogen flame.

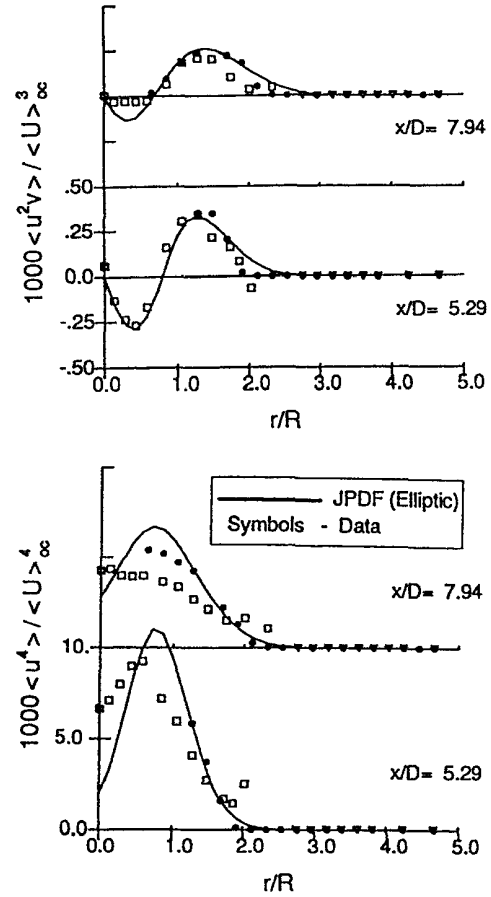


Figure 7: Computed profiles of higher-order turbulent correlations compared against data for the hydrogen flame.

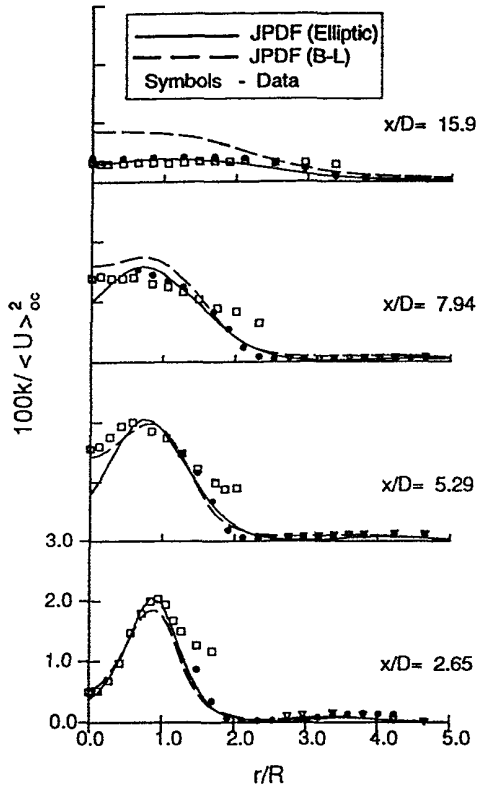


Figure 6: Computed turbulent kinetic energy profiles compared against data for the hydrogen flame.

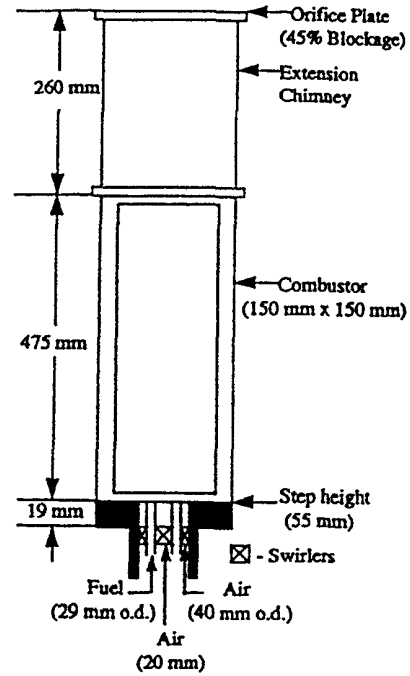


Figure 8: Schematic of the step-swirl combustor. The fuel used is methane.

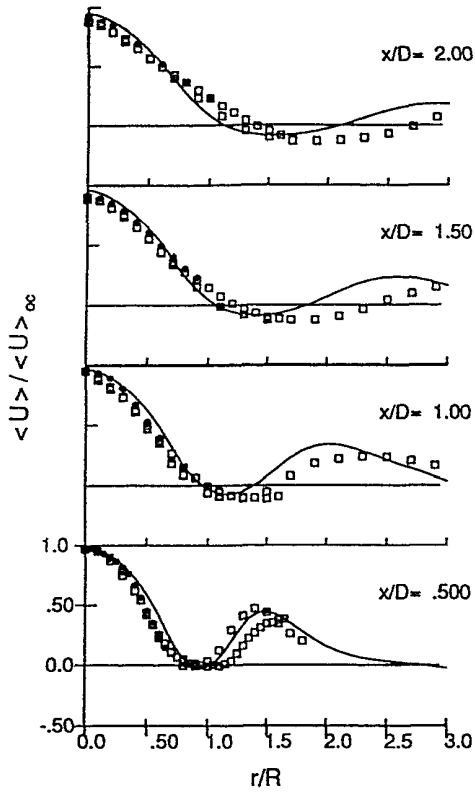


Figure 9: Computed mean axial velocity profiles (lines) compared against data (symbols) for the methane flame.

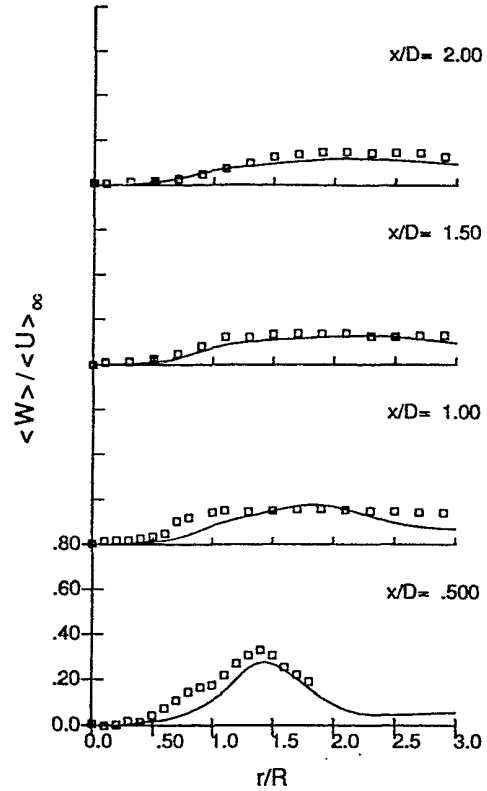


Figure 11: Computed mean swirl velocity profiles (lines) compared against data (symbols) for the methane flame..

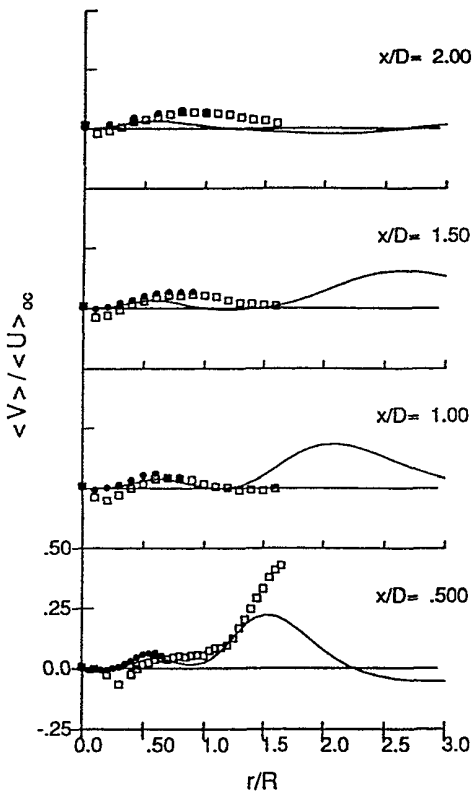


Figure 10: Computed mean radial velocity profiles (lines) compared against data (symbols) for the methane flame.

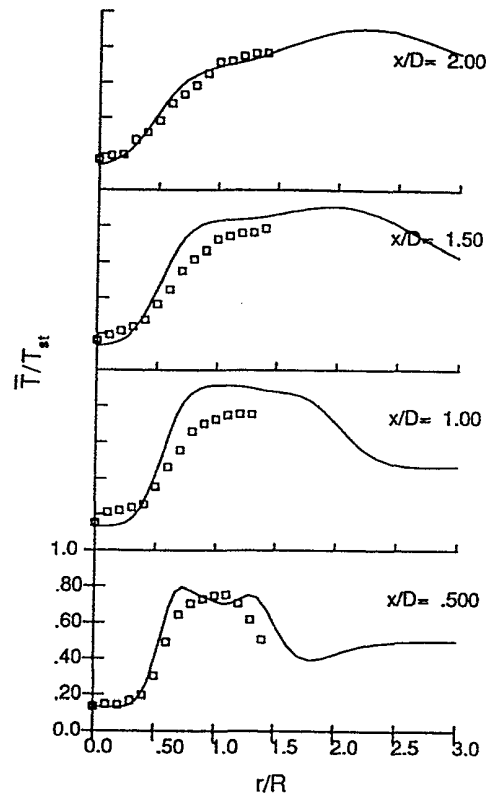


Figure 12: Computed mean temperature profiles (lines) compared against data (symbols) for the methane flame.

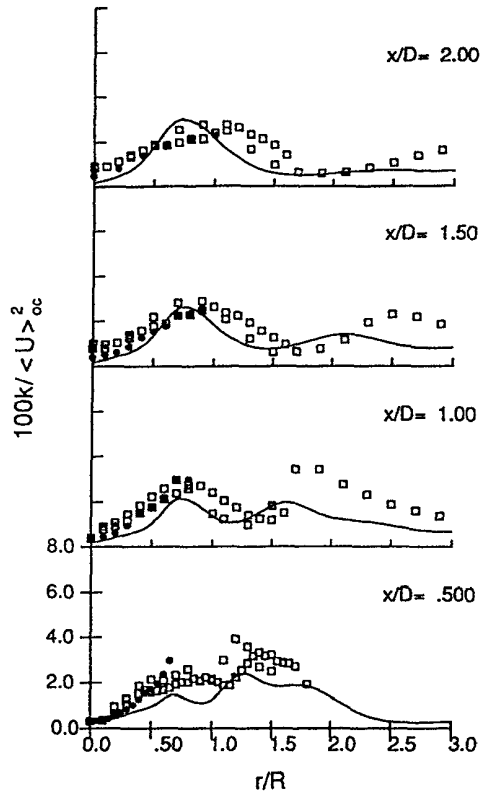


Figure 13: Computed turbulent kinetic energy profiles (lines) compared against data (symbols) for the methane flame.

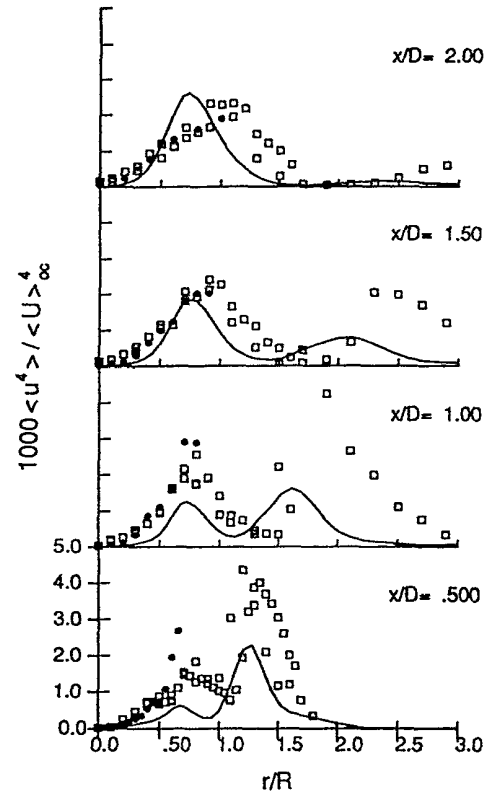


Figure 14: Computed profiles of fourth moment of axial velocity (lines) compared against data (symbols) for the methane flame